Higgs pair production in the four b quarks final state

Ana Luísa Moreira de Carvalho

Instituto Superior Técnico, Lisboa, Portugal

December 2011

Abstract

Place abstract here. No paragraph breaks.
Keywords: Keyword1, Keyword2, Keyword3, Keyword4, Keyword5

1. Introduction and motivation

A lot of work as is currently being put into designing and understanding the physics reach of future particle colliders. The hadronic Future Circular Collider (FCC-hh) study, led by CERN, is one of the possibilities that is currently being analyzed. Its baseline design consist of a 100 km ring located in the Geneva area capable of delivering proton-proton collisions at a center of mass energy of 100 TeV. The FCC-hh will deliver a peak luminosity of $\mathcal{L} = 30 \times 10^{34} \mathrm{cm}^{-2}\mathrm{s}^{-1}$ in its ultimate phase. This will result in $O(30)$ ab^{-1} per experiment. The next milestone for this project is the delivery of a Conceptual Design Report (CDR) by the end of 2018. This document should include a first cost estimate as well as a compilation of preliminary analysis that illustrate the physics potential of such an accelerator.

A particularly interesting process to be studied in future colliders is the production of pairs of Higgs bosons (or di-Higgs production). This process is sensitive to the value of the Higgs boson triple coupling that determines the shape of the Higgs potential and therefore plays a crucial role in the electroweak symmetry breaking mechanism. The Feynamn diagram that provides sensitivity to the triple coupling is shown in figure 1.

However, searches for di-Higgs production are extremely challenging mainly because the cross section of this process is very small, of the order of tens of femtobarns (fb). Even with the entire dataset that is expected to be accumulated during the LHC's (including its high luminosity upgrade) lifetime ($O(3)$ ab^{-1}), it is very unlikely that we will be able to declare the observation of this process. Therefore, the discovery of di-Higgs production relies on future colliders making it a key benchmark process.

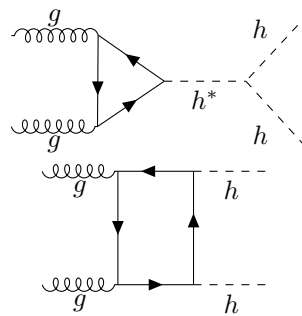In this work we focus on the final state with four b quarks. The branching ratio (BR) of $h \to b\bar{b}$ is

Figure 1: Feynman diagrams for the $gg \to hh$ process at leading order.

approximately 58%. Therefore this final state maximizes the cross section times branching of the $hh \to b\bar{b}b\bar{b}$ process. However, for this final state, the dominant background is multijet production through quantum chromodynamics (QCD) processes whose cross section is a lot larger than that of the signal. Nonetheless, it is a well known characteristic of QCD interactions that the partons (and jets) produced tend to a low transverse momentum (p_T). This indicates that exploring a high p_T region of the phase space could be the key to suppress the QCD multijet background. Such region is called boosted due to the high Lorentz boost of the objects involved. In this kinematic regime, traditional jet reconstruction algorithms, that establish a one to one correspondence between the partons and the jets, begin to fail because the ΔR distance between the b quarks, $\Delta R(b\bar{b})$, gets increasingly smaller as the p_T of the mother Higgs boson, $p_T(h_1)$, increases. This is shown in figure 1. State of the art jet reconstruction techniques use a single jet with a large R parameter to reconstruct both b quarks as a single jet that is used as a *proxy* for the Higgs boson. In order to extract as much information as possible from this jets it is important to analyze its intrinsic structure, referred to as substructure. Such techniques

1

are fairly recent and usually explore the existence of well defined energy maximums inside a large R jet. For example, a jet that contains the two b quarks coming from the decay of a Higgs boson is expected to be more compatible with the existence of two subjets than a jet produced by a QCD process.
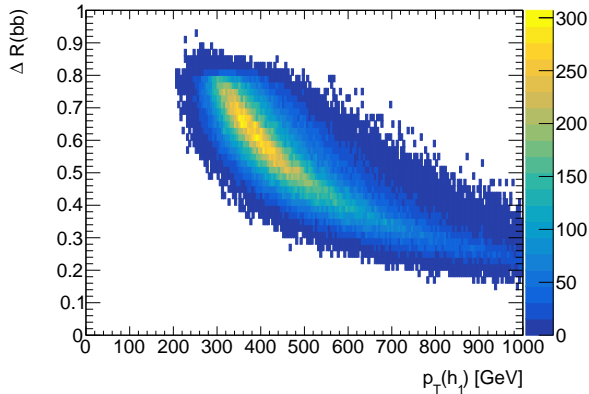

Figure 2: oi

From the point of view of detector design for the FCC-hh, as well as for future upgrades of existent detectors such as the ATLAS one, the granularity of the hadronic calorimeter (HCAL) is a key parameter because it greatly influences the ability of the detector to resolve the substructure of large R jets.

The main goal of this project is to use boosted di-Higgs production in the four b quarks final state to study the influence of the granularity of the HCAL in the significance $(S/\sqrt{B})$ that can be achieved.

2. Collider experiments
2.1. The LHC and the ATLAS detector
The Large Hadron Collider (LHC) is housed by the European Organization for Nuclear Reasearch (CERN) and located beneath the Franco-Swiss boarder in the Geneva area. It consists of a 27 km ring dedicated (most of the time) to delivering proton-proton collisions at a center of mass (CM) energy of $\sqrt{s} = 13$ TeV. The two main purpose experiments, ATLAS and CMS, are dedicated to the search for any hints of new physics. The LHCb experiment is dedicated to the study of beauty particles and the ALICE experiment is optimized to study heavy ion collisions.

The ATLAS detector is a multipurpose particle physics apparatus with forward-backward symmetric cylindrical geometry. The inner tracking detector (ID) consists of a silicon pixel detector, a silicon microstrip detector, and a straw-tube transition radiation tracker. It is contained in a superconducting solenoid magnet that provides a 2 T magnetic field and surrounded by a high-granularity liquid-argon sampling electromagnetic calorimeter (ECAL). The

ECAL covers the pseudo-rapidity range $|\eta| < 3.2$. The hadronic calorimetry in the pseudorapidity range $|\eta| < 1.7$ is provided by a scintillator-tile calorimeter (TileCal). For $|\eta| > 1.5$ liquid-argon calorimeters extend the pseudorapidity range to $|\eta| = 4.9$. The LAr calorimeter is divided in end-cap and forward. These cover the pseudorapidity ranges $1.5 < |\eta| < 3.2$ and $3.2 < |\eta| < 4.9$. In the end-cap the segmentation is $\Delta\eta \times \Delta\phi = 0.1 \times 0.1$ for $1.5 < |\eta| < 2.5$ and 0.2×0.2 for $2.5 < |\eta| < 3.2$. In the forward region the segmentation is $\Delta\eta \times \Delta\phi = 0.2 \times 0.2$. The muon spectrometer (MS) surrounds the calorimeters and it is the outermost layer of the detector. It is composed of Monitored Drift Tubes and Cathode Strip Chambers.

2.2. The FCC-hh
The FCC-hh baseline design consist of a of a proton-proton circular collider with a maximum CM energy of $\sqrt{s} = 100$ TeV housed by a 100 km tunnel in the area of Geneva. It will deliver a peak luminosity of $\mathcal{L} = 30 \times 10^{34}$ cm^{-2}s^{-1} in its ultimate phase which will result in a $O(30)$ ab^{-1} per experiment. This machine will extend the research program of the LHC (and of the HL-LHC) after these have reached their full discovery potential, by around 2040.

The design of the FCC-hh baseline detector has been greatly based on that of the ATLAS and CMS experiments, in particular the central barrel. The layers and sub detectors are arranged in the same order and perform very similar roles. The ID detector covers the pseudorapidity range $|\eta| < 6$ and it will be instrumented with pixel and strip detectors. The ECAL covers the pseudorapidity range $|\eta| < 6$. The proposed layout is a LAr sampling configuration with lead, glue and steal plates as absorbers. The granularity is expected to be two to four times better than for the ATLAS ECAL. The hadronic calorimeter covers the pseudorapidity range $|\eta| < 6$. It is divided in barrel, end-cap and forward that cover the pseudorapidity ranges $|\eta| < 1.3$, $1.0 < |\eta| < 1.8$ and $2.3 < |\eta| < 6.0$. For the barrel and end-cap calorimeters, the expected segmentation $\Delta\eta \times \Delta\phi = 0.025 \times 0.025$ while for the forward calorimeter it is $\Delta\eta \times \Delta\phi = 0.05 \times 0.05$. Overall, this corresponds to approximately four times the ATLAS HCAL granularity. The MS cover the pseudorapidity range $|\eta| < 6$ and it consists of a layered structure of gas chambers.

3. State of the art
The searches performed so far for di-Higgs production covered different decay channels and targeted not only the SM production but also some BSM scenarios where this process is enhanced. Neither could achieve enough statistical significance to declare the observation of this process nor found any deviation from the SM predictions.

The most stringent limit comes from a combination of searches using up to 36.1 fb^{-1} of proton-proton collision data at a center of mass energy $\sqrt{s} = 13$ TeV recorded with the ATLAS detector [1]. The combination is performed using the analysis searching for $hh \to b\bar{b}b\bar{b}$, $hh \to b\bar{b}\tau^+\tau^-$ and $hh \to b\bar{b}\gamma\gamma$. The combined observed (expected) limit on the non-resonant Higgs boson pair cross-section is 0.22 pb (0.35 pb) at 95% confidence level, which corresponds to 6.7(10.4) times the predicted SM cross-section. The ratio of the Higgs boson self-coupling to its SM expectation ($k_\lambda = \lambda_{hhh}/\lambda_{hhh}^{SM}$) is observed (expected) to be contrained at 95% CL to $-5.0 < k_\lambda < 12.1(-5.8 < k_\lambda < 12.0)$.

Monte Carlo studies assessing the feasibility of searches for di-Higgs production at the High Luminosity LHC (HL-LHC) and at the FCC-hh have been performed. For the HL-LHC, a study including the $pp \to b\bar{b}b\bar{b}$, $pp \to b\bar{b}jj$, $pp \to jjjj$ and $pp \to t\bar{t}jjjj$ reports a significance of $S/\sqrt{B} = 3.1$ (1.0) for an integrated luminosity of 3000 (300) fb^{-1}, considering a mean pileup of 80 [2]. The analysis is performed in three orthogonal signal categories (resolved, intermediate and boosted) and the reported significance is obtained from the combination of the three regions. This study makes use of an artificial neural network to further increase the signal-background separation. Similar studies performed by ATLAS and CMS find the $hh \to b\bar{b}\gamma\gamma$ channel to be the most sensitive to the Higgs trilinear coupling. ATLAS reports a significance of 1.06 for an integrated luminosity of 3000 fb^{-1}, which translates to a 95% CL limit on the ratio of the Higgs boson self-coupling to its SM expectation of $-0.8 < k_\lambda < 7.7$ [3]. This analysis is purely cut based and a mean pileup of $<\mu> \sim 200$ is considered.

For the FCC-hh, a recent study simulates the signal with an extra jet at generator level: $pp \to b\bar{b}b\bar{b}j$ [4]. The extra jet boosts the Higgs pair favoring a highly boosted virtual Higgs decaying to a pair of Higgs bosons which enhances the sensitivity to the Higgs trilinear coupling. Only the irreducible background, $pp \to b\bar{b}b\bar{b}j$, is considered. A significance of 6.61 is reported for an integrated luminosity of 30 ab^{-1}. No MVA techniques are applied nor pileup contribution considered.

Studies on the impact of the granularity of the calorimeters in the spatial resolving power of hadronic showers and on the resolution of jet mass and substructure variables greatly influenced the baseline design of the FCC-hh. For two Kaons with an energy of 100 GeV each and with a truth level separation equal to 0.035 it is shown that for a segmentatin of $\Delta\eta \times \Delta\phi = 0.022 \times 0.022$ both particles can be resolved in the HCAL [5]. A series of results presented in [6, 7, 8] analyze three calorimeters benchmark configura-

tions: HCAL(ECAL) $0.1(0.025)\eta \times 5.6(1.4)deg\phi$, HCAL(ECAL) $0.05(0.012)\eta \times 2.8(0.7)deg\phi$ and HCAL(ECAL) $0.025(0.006)\eta \times 1.4(0.35)deg\phi$. The jet mass resolution for jets with $p_T > 3$ TeV in $t\bar{t}$ events improves by 80% and 120% for $\Delta\eta \times \Delta\phi = 0.05 \times 0.05$ and $\Delta\eta \times \Delta\phi = 0.025 \times 0.025$ cells with respect to $\Delta\eta \times \Delta\phi = 0.1 \times 0.1$. The resolution on the τ_{32} variable is also shown to increase as the granularity increases. In addition, eflow (particle flow) jets are shown to have a better resolution than calorimeter jets. In [6] it is shown that the overlap between the distributions of the τ_{21} variable in W and QCD jets decreases from 80% to 60% going from $\Delta\eta \times \Delta\phi = 0.1 \times 0.1$ to $\Delta\eta \times \Delta\phi = 0.005 \times 0.005$. For 20 TeV jets this effect is absent.

4. Analysis
The main backgrounds affecting di-Higgs searches in the $b\bar{b}b\bar{b}$ are multijet and $t\bar{t}$ production. All other sources of background, including processes involving Higgs bosons, are found to be negligible [REF]. In addition to these, we also consider the irreducible background as a separate background source.

We study the production of Higgs pairs in three different models: the SM, a dark matter model with a 1 TeV spin-0 mediator that can decay to Higgs pairs and the CP-conserving 2HDM of type II where the heavier CP-even Higgs can decay to pairs of SM Higgs bosons.

We choose the mass of the new heavy resonances to be high (~ 1 TeV) in order to increase the efficiency of the boosted selection.

4.1. Simulation setup
We simulate the signal and background Monte Carlo samples using a fast simulation workflow. MadGraph5 aMC@NLO [9] is used to compute the matrix elements of a given process. Showering and hadronization of colored particles are handled by Pythia8 [10] and the detector response is parameterized using Delphes3 [11].

The irreducible background is generated with an extra jet with $p_T > 200$ GeV at generator level ($4b + j$). This guarantees that the pairs of b quarks are boosted enough to increase the probability of being reconstructed as a single jet. The multijet background is simulated as $jj + 0/1/2\ j$ where j stands for a light or b jet. To make the simulation more efficient, this background is generated in several H_T regions between $500 < H_T < 100000$, where H_T is the scalar sum of the p_T of all the partons at generator level. The $t\bar{t}$ background is simulated as $t\bar{t} + 0/1/2\ j$. The sample is inclusive in the top quark and $W^\pm$ boson decay modes.

The BSM signal samples are simulated using publicly available in the FeynRules database. For the DM mediator model [12], the spin-0 mediator mass

is set at 1 TeV.The cross section for the signal generated with this model is smaller than the cross section of the SM signal (approximately 0.2 pb versus 0.7 pb) and therefore this model is not excluded by experimental data.

For the 2HDM [13, 14], the input parameters for the scalar sector are: the mass of the scalars and charged bosons, $m_{h_1} = 125$ GeV, $m_{h_2} = 900$ GeV, $m_{h_3} = 850$ GeV and $m_{h_c} = 800$ GeV, the mixing between the scalars, $mix_{h_2} = mix_{h_3} = 0$ and $mix_h = \frac{\pi}{2} - (\beta - \alpha)$ where we have chosen $\beta = \frac{\pi}{4}$ and $\alpha = -0.75$, and the quartic couplings of the potential, $l_2 \simeq 0.27$, $l_3 \simeq 9.46$ and $l_7 \simeq 0.46$. All parameters are given in the Higgs basis. Regarding the Yukawa sector, we consider the type II model. The real part of the Yukawa matrices of the coupling of h_2 to down (GDR) and up-type (GUR) quarks are given by [13]: $GDR = \mathrm{diag}\left(0, 0, \frac{m_b \sqrt{2}\tan(\beta)}{v}\right)$ and $GUR = \mathrm{diag}\left(0, 0, \frac{m_b \sqrt{2}}{v \tan(\beta)}\right)$, where $m_b = 4.7$ GeV and $m_t = 172$ GeV are the masses of the bottom and top quarks. All other matrices are null.

Different detector configurations were implemented in Delphes3. The granularity of the HCAL was the main study parameter. Starting from the FCC-hh baseline detector, five HCAL granularity benchmark configurations were tested:

1. ATLAS HCAL granularity;

2. Starting from the ATLAS HCAL configuration we increase the granularity in $|\eta|$ by four, in the pseudorapidity range $|\eta| < 1.7$ which corresponds to the TileCal region;

3. Starting from the FCC HCAL configuration we decrease the granularity in by two, in the entire pseudorapidity range covered by the HCAL;

4. FCC HCAL default granularity;

5. Starting from the FCC HCAL configuration we increase the granularity in $|\eta|$ and in ϕ by two, in the entire pseudorapidity range covered by the HCAL.

These configurations are summarized in table 1. In addition, we also passed the same generator level samples through the default ATLAS detector simulation in Delphes. The HCAL granularity is the one that is indicate in the first line of table 1 but the other detectors parameters, such as the radius, magnetic field, tracking resolutions are the ones that are implemented in the default ATLAS Delphes card.

4.2. Event selection

This targets the boosted kinematic regime in which both Higgs bosons are reconstructed using large R

Config.	$\Delta\eta \times \Delta\phi$	η range
1	0.1×0.1	$\|\eta\| < 2.5$
	0.2×0.2	$2.5 < \|\eta\| < 5.0$
2	0.025×0.1	$\|\eta\| < 1.7$
	0.1×0.1	$1.7 < \|\eta\| < 2.5$
	0.2×0.2	$2.5 < \|\eta\| < 5.0$
3	0.025×0.05	$\|\eta\| < 2.5$
	0.05×0.1	$2.5 < \|\eta\| < 6.0$
4	0.025×0.025	$\|\eta\| < 2.5$
	0.05×0.05	$2.5 < \|\eta\| < 6.0$
5	0.0125×0.0125	$\|\eta\| < 2.5$
	0.025×0.025	$2.5 < \|\eta\| < 6.0$

Table 1: Summary of the benchmark granularity configurations of the HCAL.
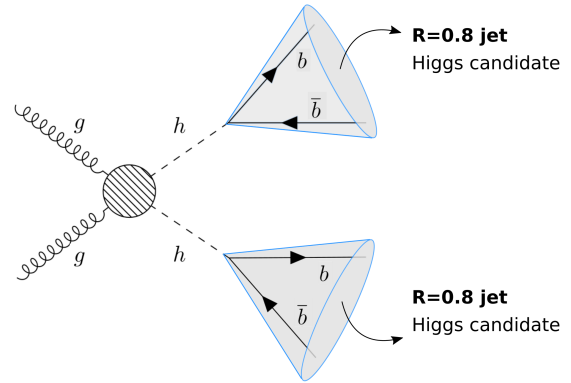

Figure 3: oi

jets. The expected event topology is illustrated in figure 4.2.

The events are reconstructed using particle flow (or calorimeter) jets with $R = 0.8$ clustered with the anti-k_T algorithm. The events are required to have at least two jets. Each jet is required to have two subjets, both b-tagged. In addition, both jets are required to have $p_T > 200$ GeV. These cuts consist of the event pre-selection.

The b-tagging is implemented using truth level information. The b-tagging and mis tagging efficiencies are extracted from the FCC-hh detector default Delphes card, implemented by the FCC-hh study group.

The event selection is described in the following paragraphs. The value of the cuts follow from a scan over all the possible cut values. We choose the cut value that maximizes the significance, $S/\sqrt{B}$.

We require

$$p_T(h_1) > 300 \text{ GeV}, \quad p_T(hh) > 100 \text{ GeV} \quad (1)$$

where $p_T(h_1)$, $p_T(hh)$ are the transverse momentums of the leading Higgs candidate and of the

pair of Higgs candidates. These cuts help suppress multijet background whose p_T distributions fall more steeply than for the signal. A requirement on the maximum value of the N-subjetiness variable of the leading and subleading Higgs candidates, $\tau_{21}(h_1, h_2)$ to further reject jets that are not consistent with a two-prong substructure:

$$\tau_{21}(h_1, h_2) < 0.4. \tag{2}$$

These cuts work as a Higgs tagging criteria. Since high-mass resonances tend to produce more central jets than multijet background processes we require

$$|\eta(hh)| < 1.5. \tag{3}$$

We place an additional requirement on the second Fox Wolfram momentum of the leading Higgs candidate, $H_2(h_1)$, to further suppress $t\bar{t}$ contamination

$$H_2(h_1) < 0.2. \tag{4}$$

Events are selected if the soft drop masses, M_{SD}, of the large-R jets are consistent with the SM Higgs boson mass

$$(100 < M_{SD}(h_1, h_2) < 135) \text{ GeV.} \tag{5}$$

5. Results

The analyses described in section 4 was developed and optimized using samples simulated with the default FCC-hh detector implementation. The results are reported in terms of the significance, $S/\sqrt{B}$, that was achieved (section 5.1). The same analysis is applied to the different detector configurations (describe in section 4.1) and the results compared in terms of significance and singnal efficiency (section 5.2).

5.1. Higgs pair discovery potential at the FCC-hh

Considering the SM signal production the achieved significance is

$$(S/\sqrt{B})_{SM} = 6.8 \pm 0.7 \ (2.15 \pm 0.27) \text{ [UPDATE]} \tag{6}$$

for an integrated luminosity of 30 (3) ab^{-1}. For the 1 TeV DM mediator signal, the significance is 1.48 ± 0.15 (0.47 ± 0.05) for an integrated luminosity of $\mathcal{L} = 30$ (3) ab^{-1} which make a not so interesting model from the point of view of enhancing Higgs pair production. For the 2HDM signal the achieved significance is

$$(S/\sqrt{B})_{2HDM} = 8.7 \pm 0.9 \ (2.76 \pm 0.28) \text{ [UPDATE]} \tag{7}$$

for $\mathcal{L} = 30$ (3) ab^{-1}.

The signal efficiency is higher for both BSM models than for the SM because the masses of

the new heavy resonances were chosen to be large ($O(1 \text{ TeV})$) to produce highly boosted Higgs pairs. For the SM the efficiency is 0.422%. It increases to 0.487% for the DM mediator model and to 1.342 for the 2HDM.

5.2. Granularity studies for future colliders

Figure 5.2 shows the signal efficiency (in percentage) as a function of the detector configuration. The left most point corresponds to the ATLAS detector and the right most point to the FCC-hh detector with a granularity twice as good in η and ϕ (configuration 5 in table 1). The points in between are ordered by increasing granularity of the HCAL. All other plots that show some quantity as a function of detector configuration follow the same convention. For all signal models, the efficiency increases as the granularity of the HCAL increases. [QUANTIFY INCREASE IN PERCENTAGE].

Figures 5.2 and 5.2 show the significance ($S/\sqrt{B}$) as a function of the detector configuration for the SM signal model and for the 2HDM, respectively. Triangular markers represent analysis that were performed using pure HCAL jets while square markers represent analysis performed using energy flow jets. The expected significance is shown for $\mathcal{L} = 30$ ab^{-1} (filled markers) and for $\mathcal{L} = 30$ ab^{-1} (empty markers).

With the exception of some fluctuations, the significance increases as the granularity increases. For energy flow jets the change in significance is very mild. [QUNATIFY] It becomes more pronounced when using pure calorimeter jets. [QUANTIFY] However, when using calorimeter jets, the achieved significance is always smaller because we are not using information from the tracking system. This is verified for both the SM and 2HDM signals. These results indicate that when using energy flow jets the tracking system is dominating the reconstruction in terms of energy resolution.

6. Conclusions

Conclusions, future work and some final remarks...

Acknowledgements

References

[1] A. Collaboration, Combination of searches for Higgs boson pairs in pp collisions at 13 TeV with the ATLAS experiment., Tech. Rep. ATLAS-COM-CONF-2018-048, CERN, Geneva (Aug 2018).
URL https://cds.cern.ch/record/2634999

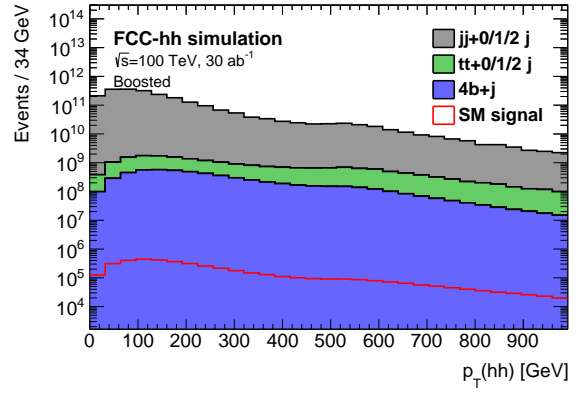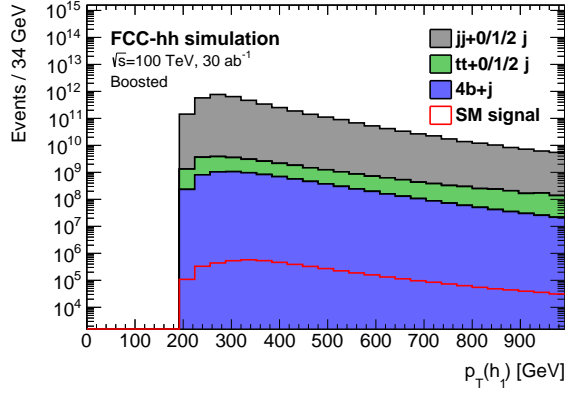[2] J. K. Behr, D. Bortoletto, J. A. Frost, N. P. Hartland, C. Issever, J. Rojo, Boosting Higgs pair production in the $b\bar{b}b\bar{b}$ final state with multivariate techniques, Eur. Phys.
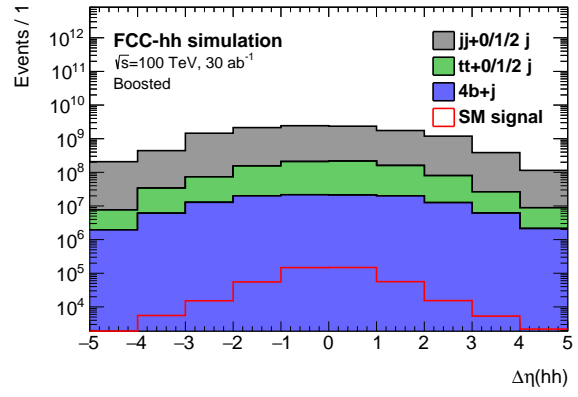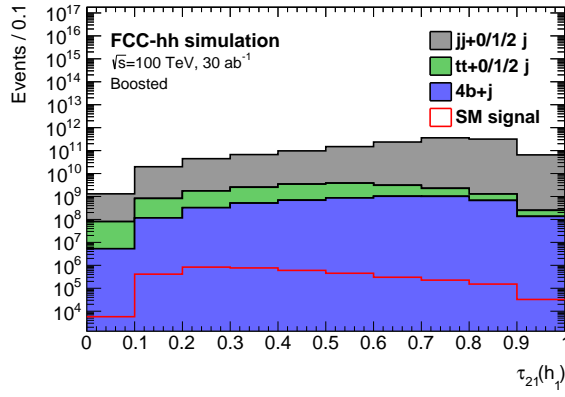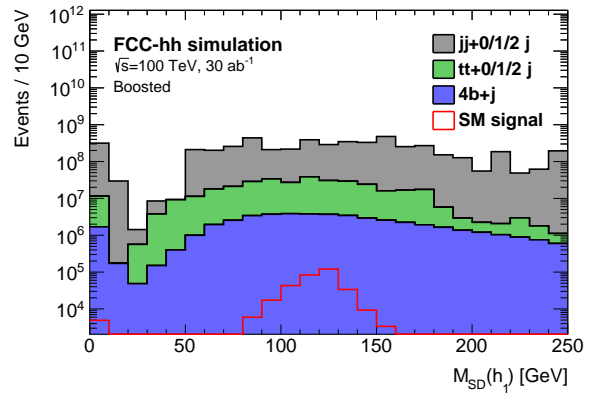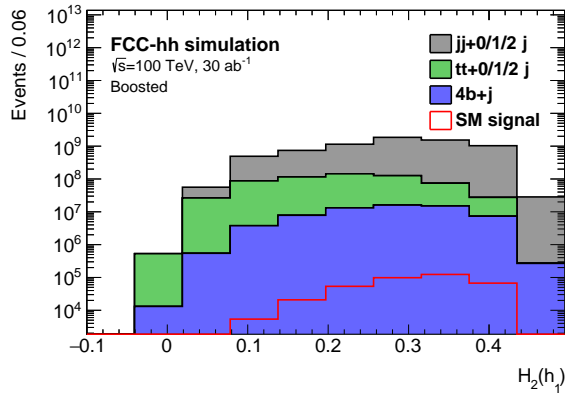
Figure 4: oi

Figure 5: oi

Figure 6: oi
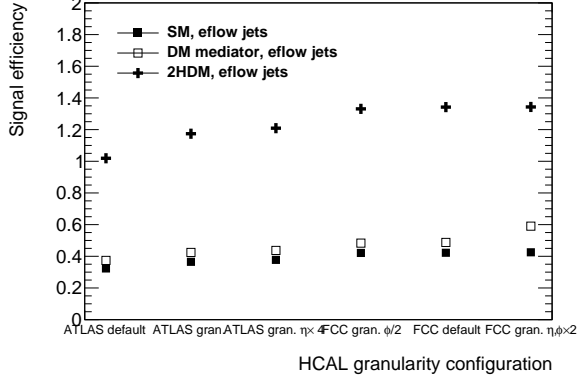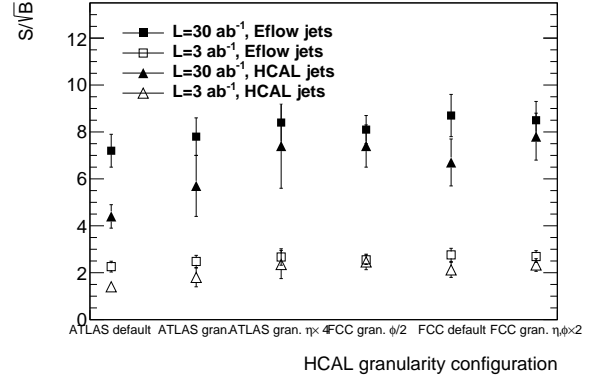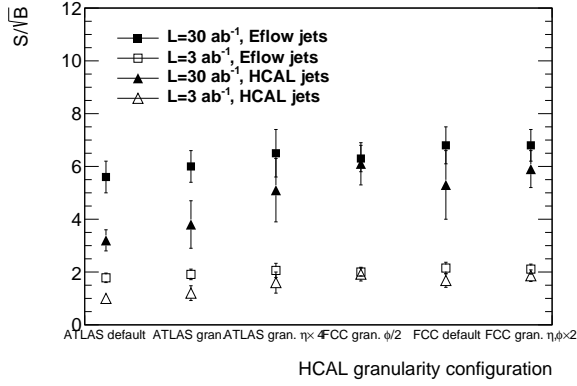
Figure 7: oi

Figure 9: oi

Figure 8: oi

J. C76 (7) (2016) 386. arXiv:1512.08928, doi:10.1140/epjc/s10052-016-4215-5.

[3] Study of the double Higgs production channel $H(\to b\bar{b})H(\to \gamma\gamma)$ with the ATLAS experiment at the HL-LHC, Tech. Rep. ATL-PHYS-PUB-2017-001, CERN, Geneva (Jan 2017). URL https://cds.cern.ch/record/2243387

[4] S. Banerjee, C. Englert, M. L. Mangano, M. Selvaggi, M. Spannowsky, hh + jet production at 100 TeV, Eur. Phys. J. C78 (4) (2018) 322. arXiv:1802.01607, doi:10.1140/epjc/s10052-018-5788-y.

[5] S. V. Chekanov, M. Beydler, A. V. Kotwal, L. Gray, S. Sen, N. V. Tran, S. S. Yu, J. Zuzelski, Initial performance studies of a general-purpose detector for multi-TeV physics at a 100 TeV pp collider, JINST 12 (06) (2017) P06009. arXiv:1612.07291, doi:10.1088/1748-0221/12/06/P06009.

[6] S. Chekanov, Boosted jets in high-granularity calorimeter at a 100 TeV pp collider, bOOST 2017 (2017).

[7] S. Chekanov, Physics requirements for a Hadron Calorimeter for a 100 TeV proton-proton collider, fCC week 2015 (2015).

[8] S. Chekanov, Simulation of a high-granular hadronic calorimeter for multi-TeV physics, fCC week 2016 (2016).

[9] J. Alwall, M. Herquet, F. Maltoni, O. Mattelaer, T. Stelzer.

[10] T. Sjostrand, S. Mrenna, P. Z. Skands, A Brief Introduction to PYTHIA 8.1, Comput. Phys. Commun. 178 (2008) 852–867. arXiv:0710.3820, doi:10.1016/j.cpc.2008.01.036.

[11] J. de Favereau, C. Delaere, P. Demin, A. Giammanco, V. Lematre, A. Mertens, M. Selvaggi, DELPHES 3, A modular framework for fast simulation of a generic collider experiment, JHEP 02 (2014) 057. arXiv:1307.6346, doi:10.1007/JHEP02(2014)057.

[12] H. C. van de Hulst, E. Raimond, H. van Woerden, Rotation and density distribution of the Andromeda nebula derived from observations of the 21-cm line 14 (1957) 1.

[13] T. general Two-Higgs-Doublet Model, C. degrande, c. duhr, m. herquet (2018). URL http://feynrules.irmp.ucl.ac.be/wiki/2HDM

[14] C. Degrande, Automatic evaluation of UV and R2 terms for beyond the Standard Model Lagrangians: a proof-of-principle, Comput. Phys. Commun. 197 (2015) 239–262. arXiv:1406.3030, doi:10.1016/j.cpc.2015.08.015.